

## Spectacular *Spitzer* Images of the Trifid Nebula: Protostars in a Young, Massive-star-forming Region

Jeonghee Rho and William T. Reach

*Spitzer Science Center, California Institute of Technology, Pasadena, CA 91125;*  
*rho@ipac.caltech.edu, reach@ipac.caltech.edu*

Bertrand Lefloch

*Laboratoire d'Astrophysique, Observatoire de Grenoble, BP 53, F-38041, Grenoble CEDEX9,*  
*France; lefloch@obs.ujf-grenoble.fr*

Giovanni G. Fazio

*Harvard-Smithsonian Center for Astrophysics, MS 42, 60 Garden Street, Cambridge, MA 02138;*  
*gfazio@cfa.harvard.edu*

### ABSTRACT

*Spitzer* IRAC and MIPS images of the Trifid Nebula (M20) reveal its spectacular appearance in infrared light, highlighting the nebula's special evolutionary stage. The images feature recently-formed massive protostars and numerous young stellar objects, and a single O star that illuminates the surrounding molecular cloud from which it formed, and unveil large-scale, filamentary dark clouds. The hot dust grains show contrasting infrared colors in shells, arcs, bow-shocks and dark cores. Multiple protostars are detected in the infrared, within the cold dust cores of TC3 and TC4, which were previously defined as Class 0. The cold dust continuum cores of TC1 and TC2 contain only one protostar each; the newly discovered infrared source in TC2 is the driving source of the HH399 jet. The *Spitzer* color-color diagram allowed us to identify  $\sim 160$  young stellar objects (YSOs) and classify them into different evolutionary stages. The diagram also revealed a unique group of YSOs which are bright at  $24\mu\text{m}$  but have the spectral energy distribution peaking at  $5\text{-}8\mu\text{m}$ . Despite expectation that Class 0 sources would be "starless" cores, the *Spitzer* images, with unprecedented sensitivity, uncover mid-infrared emission from these Class 0 protostars. The mid-infrared detections of Class 0 protostars show that the emission escapes the dense, cold envelope of young protostars. The mid-infrared emission of the protostars can be fit by two temperatures of 150 and 400 K; the hot core region is probably optically thin in the mid-infrared regime, and the size of hot core is much smaller than that of the cold envelope. The presence of multiple protostars within the cold cores of Class 0 objects implies that

clustering occurs at this early stage of star formation. The TC3 cluster shows that the most massive star is located at the center of the cluster and at the bottom of the gravitational-potential well.

*Subject headings:* Stars: formation - infrared:Stars – ISM: individual (Trifid Nebula) – ISM:HII regions

## 1. Introduction

The Trifid Nebula (M20), is one of the best-known astrophysical objects: a classical nebula of ionized gas from an O7 star (HD 164492). The nebula glows in red light, trisected by obscuring dust lanes, with a reflection nebula in the north. The Trifid Nebula is a very young H II region with an age of  $\sim 3 \times 10^5$  years. The Infrared Space Observatory (ISO) and the Hubble Space Telescope (HST) (Cernicharo et al. 1998; Lefloch & Cernicharo 2000; Hester et al. 1999) show the Trifid to be a dynamic, “pre-Orion” star forming region containing young stellar objects (YSOs) undergoing episodes of violent mass ejection, and protostars (like HH399) losing mass and energy to the nebula in jets. Four massive (17–60  $M_{\odot}$ ) protostellar cores were discovered, with millimeter-wave observations, in the Trifid (Lefloch & Cernicharo 2000). A number of YSO candidates were identified using near-infrared (Rho et al. 2001) and X-ray observations (Rho et al. 2004). We adopted a distance of 1.68 kpc for the Trifid Nebula, which was measured by Lynds et al. (1986). There have been two primary tools for studying massive star formation: molecular line emission which traces dense material and outflows (e.g. Shirley et al. 2003), and dust continuum emission which traces cold, dense material (e.g. William et al. 2004). The youngest objects, Class 0 protostars, are those that are detected as condensations in dust continuum maps characterized by very low values of the ratio  $L_{bol}/L_{submm}$ , and show collimated CO outflows or internal-heating sources (André 1994). The Class 0 protostars were believed to be “starless” cores, with neither near-infrared nor mid-infrared ( $<20\mu\text{m}$ ) emission. In this paper, we present spectacular *Spitzer* images of the Trifid Nebula and report  $\sim 160$  newly identified young stellar objects (YSOs) using their infrared colors. We found multiple protostars within cold cores and many evolved YSOs are located along the ionization fronts. We illustrate that *Spitzer* infrared images provide new, excellent tools for studying massive-star formation in ways that were not previously available.

## 2. Observations

We performed our infrared observations of the Trifid Nebula with the *Spitzer* Space Telescope, the fourth NASA Great Observatory. The Infrared Array Camera (IRAC; Fazio et al. 2004) and Multiband Imaging Photometer for *Spitzer* (MIPS; Rieke et al. 2004) observations took place on March 31, 2004 (AOR = 6049024) and April 11, 2004 (AOR = 6048768), respectively. The integration time is 8 seconds for IRAC and 48 seconds for MIPS per sky position. The data are

processed with the *Spitzer* Science Center (SSC) pipeline<sup>1</sup>. For individual frame data known as “Basic Calibrated Data” (BCD), outlier rejection was applied to remove cosmic rays, and dark and flat fields were also applied. The full-width-half-maximum (FWHM) of the point-spread-function (PSF) is approximately 1.7'' in the IRAC images and 6'' in the MIPS 24 $\mu$ m image. The uncertainty of the calibration is less than 5% for all IRAC wavelengths and less than 10% for the MIPS 24 $\mu$ m. The photometry for the sources was performed using aperture photometry, IRAF APPHOT (we used aperture sizes of 4'', 4'', 5'', 6'' and 14.7'' for IRAC bands 1, 2, 3, 4 and MIPS 24 $\mu$ m, respectively) and the photometric errors are less than 0.1 mag; when the sources are located at bright diffuse emission, the photometric uncertainty are higher. The zero-magnitude flux densities are 280.9, 179.7, 115.0, 64.13 Jy for IRAC bands 1, 2, 3, and 4, respectively (Reach et al. 2005), and 7.15 Jy for MIPS 24 $\mu$ m. The number of extracted sources (S/N > 5) is 21,400 at 3.6 $\mu$ m, 2,665 at 8 $\mu$ m, and 541 at 24 $\mu$ m.

We also performed follow-up near-infrared observations using the Palomar 200-inch Wide-infrared Camera (WIRC). The data were taken on Aug 23-26, 2004 and the exposure time was 60 sec per sky position. The sensitivities in near-infrared observations are  $\sim$ 20.0 mag for J and H bands and  $\sim$ 17 mag for K<sub>s</sub> band. The photometry at all wavelengths was merged into a catalog for sources detected at 8 $\mu$ m.

### 3. *Spitzer* infrared images and the color-color diagram

The *Spitzer* IRAC and MIPS images of the Trifid Nebula (see Figure 1) reveal its spectacular appearance in infrared light, highlighting the nebula’s special evolutionary stage. The images feature recently-formed massive protostars and numerous young stellar objects, and a single O star that illuminates the surrounding molecular cloud from which it formed, and unveil large-scale, filamentary dark clouds. The hot dust grains show contrasting infrared colors in shells, arcs, bow-shocks and dark cores. The 8 $\mu$ m emission represents polycyclic aromatic hydrocarbon (PAH) structures coinciding with the optical dust lanes and shows stripped clouds evaporating through strong UV radiation of the exciting O star, indicating that the PAH is only partially destroyed in H II regions. Numerous young stellar objects are detected as apparent color excesses in red or yellow.

By using multi-wavelength photometries, we generated the color-color diagram shown in Figure 2 and the spectral energy distributions (SEDs) of the infrared excess stars. In the color-color diagram, main sequence stars fall near (0,0) magnitudes. The protostars (Class I/0) are the reddest sources, toward the upper-right of Figure 2, and young stellar objects with disks (Class II) are intermediate. This color-color classification is based on infrared colors of YSOs (Reach et al. 2004). We also confirmed the color-color classification with the full SEDs of each category of YSOs.

---

<sup>1</sup>[http://ssc.spitzer.caltech.edu/irac\[mips\]/documents](http://ssc.spitzer.caltech.edu/irac[mips]/documents)

In the SEDs, Class I/0 SEDs rise from near-infrared to  $24\mu\text{m}$ , while Class II SEDs decrease in the near-infrared but show infrared excesses in comparison with the photosphere, as shown in Figure 3. A large population of young stellar objects is present as listed in Table 1: 37 in Class I/0, and 111 in Class II. The extinction vector is shown in the color-color diagram (Figure 2). The extinction towards Trifid is only  $A_v=1.3$  (Lynds & O’neil 1985), so it can only change the colors of  $[8]-[24]=0.04$  mag and  $[3.6]-[5.8]=0.02$  mag, which is too small to affect the classification. However, considering the local extinction towards YSOs, classification of the objects which fall at the boundaries between the Class 0/I and Class II objects in Fig. 2 may be somewhat uncertain.

A unique group of YSOs with  $[8]-[24]=1.5\sim 2.5$  and  $[3.6]-[5.8]>1.5$  appears in the *Spitzer* color-color diagram; their SEDs peak between 3 and  $8\mu\text{m}$  and typically they are bright  $24\mu\text{m}$  sources. We name them “Hot excess” young stellar objects, because of the extra, hot ( $\sim 500\text{K}$  temperature) component. We note that one of these sources is a B-type emission line star, LkH $\alpha$  124, indicating “Hot excess” stars are YSOs. The “Hot excess” stars could mostly be Herbig Ae/Be stars; such stars are believed to be the intermediate mass analogue of T Tauri stars. In order for Class II objects to be “Hot excess” YSOs, a high extinction ( $A_v>25$  mag) is required. Another possibility is the “Hot excess” YSOs are Class I/0 protostars with an extra hot component from more active accretion than typical, in addition to the cold envelope. We have noticed that the number of “Hot excess” YSOs in the Trifid Nebula is higher than those in other star-forming regions (an example is Figure 2 of Muzerolle et al. 2004); this may be related to the fact that the Trifid Nebula is in a dense star-forming environment with a high UV-radiation-field. Far-infrared observations would be needed to unambiguously identify the evolutionary stage of the “Hot excess” YSOs.

The supergiant star HD 164514, A7Iab, is responsible for the blue optical reflection nebula on the northern side of the Trifid Nebula, and is not an young stellar object. This star is located at the top left in the color-color diagram ( $[8]-[24]<1.5$  and  $[3.6]-[5.8]>1.5$ ) in the region marked as “Giants” in Figure 2; note that it is located far to the left of “Hot excess” stars. Other sources at the same location in the color-color diagram may be similar objects because of similar infrared colors. We also examined the sources with very high color excesses in  $[8]-[24]$  ( $>5$ ) but no color excess in  $[3.6]-[5.8]$  ( $=0$  to  $1.5$ ), and found that each of the objects has patches of extended emission such as reflection/emission nebulae.

We compared the distribution of YSOs in the *Spitzer* images with the cold dust continuum map (Cernicharo et al. 1998). Most of the protostars (Class I/0) are distributed along the dark filamentary cloud on the western side of M20 (see Figs. 1 and 6) and along the optical dust lanes that trisect the H II region. Most of the Class II stars, on the other hand, are distributed along the ionization fronts of the Trifid Nebula, following the circular shape of the H II region. While protostars coincide with the dust continuum cores, TC1 to TC4, they are not always precisely correlated with the dust emission peaks.

Just north of the Trifid Nebula is a region containing a surprising number of protostars (R.A.  $18^{\text{h}}02^{\text{m}}42.28^{\text{s}}$  and Dec.  $-22^{\circ}48'44.8''$ , J2000). Both the diffuse mid-infrared emission and the

distribution of young stellar objects in the  $8\mu\text{m}$  and  $24\mu\text{m}$  maps suggest that this is a small H II region with active star formation. A heating source is indicated by the presence of bright  $24\mu\text{m}$  emission from hot dust grains, and PAH-rich dust lanes surround the nebula as in the Trifid proper. We analyzed a 20cm VLA map (Yusef-zadeh et al. 2000), and adopting an electron temperature of  $10^4$  K and a recombination coefficient of  $2.7 \times 10^{-13} \text{ cm}^3 \text{ s}^{-1}$ , we found an integrated flux of 0.8 Jy and a radiative recombination rate of  $10^{47.23} \text{ s}^{-1}$ . The ionization rate is consistent with a young B0/O9.5 star or an evolved B0.5 (giant or supergiant). Hence, we suggest a massive star is hidden in the area, which implies that the region north of the Trifid Nebula proper is a separate H II region, which we named “Trifid Junior.”

#### 4. Mid-infrared Emission from Protostars and Multiple-protostars within the dust continuum cores

We identified 5 protostars within the dust continuum cores of TC3 and TC4; they are listed in Table 2 and shown in Figures 5 and 6. The *Spitzer* color-color diagram shows that most of the infrared sources are Class I/0 protostars and two sources are “Hot excess” stars. Figure 6 shows three color *Spitzer* images superposed on dust continuum contours. The TC3 and TC4 condensations have been classified as Class 0 protostellar cores. Previously, ISO observations at  $70''$  resolution implied the presence of a cold component at temperatures of  $\sim 20$  K for both TC3 and TC4 (Lefloch & Cernicharo 2000).

We constructed the spectral energy distribution of each infrared Class I/0 protostar within the TC3 and TC4 cores, from  $1.25\text{--}24\mu\text{m}$  combining the Palomar, IRAC, and MIPS  $24\mu\text{m}$  data. The luminosities are derived from the SEDs between  $1.25\text{--}24\mu\text{m}$  and are listed in Table 2. All protostars show rising SEDs from near- through mid-infrared. Figure 4 shows the SEDs of a few protostars within the TC4 and TC3 cores. The depression in the  $8\mu\text{m}$  flux relative to the apparent continuum at  $5.8$  and  $24 \mu\text{m}$ , is noticeable particularly for TC3A, TC3E, TC4A and TC4D. This is likely due to presence of deep silicate absorption. By using multi-color-temperature fits to the SEDs, we estimated the luminosities of TC4 and TC3. Here we added millimeter and  $160\mu\text{m}$  fluxes; the dust continuum sources TC4 and TC3 have millimeter fluxes of 0.6 and 0.92 Jy integrated over the half-power contours, respectively (Lefloch & Cernicharo 2000). The mid-infrared fluxes for TC3 and TC4 include the sum of TC3A-TC3C and of TC4A-TC4B, respectively, because they are within the 50% millimeter contours of TC3 and TC4 cores. We also generated the SED of TC4A, the brightest infrared source in the TC4 core, assuming a significant amount of the 1.3mm flux is from Component A. To fit this SED, we use multiple components: a cold envelope with temperature and optical depth determined by the  $160\text{--}1250\mu\text{m}$  data, and warm component mostly required by the  $24\mu\text{m}$  point, and two hot components to match the near to mid-infrared points. The warm and hot components are extinguished by the envelope, but are probably optically thin themselves (see section 5 for details). The SEDs of TC3, TC4 and TC4A, have similar best-fit temperatures of  $T_{\text{cold}} = 22$  K,  $T_{\text{warm}} = 150$  K,  $T_{\text{hot1}} = 400$  K, and  $T_{\text{hot2}} = 1300$  K. An example SED of TC4A is

shown in Figure 7. The SEDs of the TC4 and TC3 cores when adding the mid- and near-infrared fluxes, yielded total luminosities of  $\sim 1200 L_{\odot}$  and  $1700 L_{\odot}$ , respectively. This implies that the protostars are moderately massive. The estimated luminosity of TC4 falls in the range of  $500\text{--}2000 L_{\odot}$ , which was previously estimated by Lefloch & Cernicharo (2000). The near- to mid-infrared luminosities of the infrared protostars range from 1 to  $32 L_{\odot}$  as listed in Table 2. The warm and hot temperature components contribute less than a few percent of the total luminosity. However, the mid-infrared detection from the earliest protostars is new, which is important for understanding of their SEDs.

The MIPS  $24\mu\text{m}$  data points are fit by a temperature of  $\sim 150$  K; we suggest that this emission originates from the warmer, inner part of the cold envelope. Most of the IRAC data points are fit by a temperature of  $\sim 400$  K. The SEDs indicate that the protostars are hot cores within cold, dense envelopes and hot cores require internal heating. For TC4A, TC4C, and TC3D, the near-infrared emission requires a color temperature of  $\sim 1300$  K; the other sources in Table 2 have one or two band detections in the near-infrared and their SEDs do not require the presence of the 1300 K temperature component. Our detection of the extremely hot temperature of 1300 K, close to the dust sublimation temperature (the exact sublimation temperature depends on particular dust properties), is the first one from the earliest-type protostars as far as we are aware. TC4C and TC3D were classified as “Hot excess” stars so they may be in somewhat advanced stages like Class I or II. However, it is surprising to find near-infrared emission from TC4A, the brightest infrared protostar in the TC4 core, which is believed to be a Class 0 object (Lefloch et al. 2002). Some possible explanations are as follows. First, TC4A may have a star inside the envelope; in other words, nucleosynthesis may have already begun in the core. This implies that there is no clear evolutionary distinction between Class 0 and Class I. Another possibility is that the near-infrared emission is light scattered directly from the central source. Recent theoretical simulations by Indebetouw et al. (2005b) showed that near-infrared emission from protostars is a few times brighter when the envelope has a clumpy medium, due to scattered-light from the central source. When we examined our near-infrared images, we noticed that some of the protostars may have extended near-infrared emission around the point-like sources. The narrow-filter images did not show any excess emission such as in  $\text{H}_2$  and  $[\text{Fe II}]$ ; this result supports the hypothesis that the near-infrared emission may be scattered-light rather than a powering source of a jet or outflow. We also cannot rule out the possibility that near-infrared counterparts are from low mass companions. However, we favor the hypothesis that the near-infrared emission is scattered-light directly from the central source over a possibility of a star inside the cold envelope or from companions.

The mid- and near-infrared luminosities ( $L_{\text{mid-IR}}$ ) were estimated using the fits to the SEDs from 1.2 to  $24\mu\text{m}$  fluxes, as shown in Table 2. TC3A, the brightest  $24\mu\text{m}$  protostar in the TC3 core, is located in the millimeter peak and at the center of the core. However, the brightest  $24\mu\text{m}$  source in the TC4 core, TC4A, is slightly off center. The second dust continuum peak in the TC4 core (TC4b in Lefloch & Cernicharo 2000) dust continuum peak contains the *Spitzer* infrared sources of TC4D and TC4E, and has an envelope mass of  $11 M_{\odot}$  (Lefloch & Cernicharo 2000). Five protostars

in the TC4 core have mid-infrared luminosities ranging between 6-32  $L_{\odot}$ , and the protostars in the TC3 core have between 1-16  $L_{\odot}$ . This suggests that protostars within the TC3 and TC4 cores are composed of a mixture of different-mass YSOs.

In contrast to TC3 and TC4 systems, the dust continuum cores of TC1 and TC2, contain only one protostar for each, as listed in Table 2 and shown in Figure 5. The infrared protostars were identified as Class I/0 by using the color-color diagram. A heated dust shell appears around the protostar in the TC1 core, as shown in Figure 5, and the infrared shell surrounds the dark cold envelope. The images of the TC2 dust core unveil a point source lying along the axis of the HH 399 jet (see also Fig. 5) and the point source has typical protostellar colors. The SEDs of the protostars of the TC1 and TC2 infer that both bolometric luminosities are  $\sim 600 L_{\odot}$  and the mid-infrared luminosities are 19 and 24  $L_{\odot}$  for TC1 and TC2, respectively.

## 5. Discussion

The detection of multiple mid-infrared protostars from the cold dust cores is a new result. How does the mid-infrared emission leak through thick envelopes of material infalling onto the stars? Isn't the mid-infrared emission absorbed by the cold and thick envelopes? We can address where the emission arises, how the dust is heated, and how the emission escapes cold cores. The cold envelope sizes of the TC3, TC4, and TC4b cores are 0.2, 0.2, and 0.16 pc, respectively, which were determined by Lefloch & Cernicharo (2000), using the 50% contour in the millimeter flux map. The estimated optical depth is:

$$\tau_{1250} = \frac{F_{1250}}{\Omega B_{\nu}(T)} = 1.08 \times 10^{-4} F_{1250} \frac{d_{1.68kpc}^2}{R^2} \quad (1)$$

where  $F_{1250}$  is the mm-wave flux,  $\Omega$  is a solid angle of the source size,  $B_{\nu}(T)$  is a black body Planck function at a temperature of  $T$ , and  $R$  is a source radius in unit of pc. The optical depths of the TC3, TC4, and TC4b cores are between  $0.7-2.5 \times 10^{-3}$  (for a temperature of 22 K). The corresponding optical depths at  $8\mu\text{m}$  were determined using  $\tau_8 = \tau_{1250} \times (1250/8)^{\alpha_1} (8/100)^{\alpha_2}$ , where  $\alpha_1 = 2$  is the extinction slope between 100-3000 $\mu\text{m}$  and  $\alpha_2 = 1$  is the extinction slope between 10-100 $\mu\text{m}$  (Li & Draine 2001); this yields  $\tau_{8\mu\text{m}} \sim 1-7$ . The corresponding visual extinction was determined using  $A_{8\mu\text{m}}/A_K = 0.5$  (Draine 2003); this yields a total extinction of  $A_v \sim 20-150$ .

Despite the high extinction of the envelope and the high optical depth of the protostars (estimated using a temperature of 22K) at  $8\mu\text{m}$ , apparently we observed mid-IR emission from the early protostars. We note that the optical depths of 150 K and 400 K components are much smaller, more than one magnitude smaller than that of the cold (22 K) envelope. From the SED fits (see Fig. 7) we estimated that the optical depth of the  $8\mu\text{m}$  emitting region is  $< 10^{-3}$  for the warm and hot temperature components, which suggests that the accretion region is probably optically thin if it is larger than  $\sim 10$  AU. In addition, the *Spitzer* images revealed that the infrared sources of the

protostars were point-sources, inferring that the regions emitting 400 K and 150 K would be smaller than the PSF radii of the IRAC and MIPS  $24\mu\text{m}$  images, which are 0.007 pc ( $= 1500$  AU) and 0.025 pc ( $= 5 \times 10^3$  AU), respectively. This is consistent with the models of the massive protostars (Osorio et al. 1999); the cold component (responsible for far-infrared and  $1300\mu\text{m}$  emission) would be emitted from a region  $> 10^4$  AU from the central source, while the 400 K component (responsible for mid-infrared emission) would be from  $< 1500$  AU region. The mid-infrared emission can escape the dense envelope; it suffers a modest mid-infrared extinction but traces the emission directly from the accretion region. Previous ISO observations showed similarly mid-infrared counterparts of a few low mass Class 0 objects in other star forming regions (Cernicharo et al. 2000). New *Spitzer* observations of Class 0 objects also detected mid-infrared protostars in L1014 (Young et al. 2004) and Cepheus E (Noriega-Crespo et al. 2004). The detections infer that the region of hot core in early protostars is optical thin at the mid-infrared regime, and the size of hot core is smaller than the cold envelope.

The mid-infrared emission is powered by accretion of envelope material onto the protostar, and most of the bolometric luminosity at the early stage of the protostar is from accretion. The accretion rate is given by McKee & Tan (2002, 2003):

$$\begin{aligned} \dot{m}_* &= 4.75 \times 10^{-4} \epsilon_{core}^{1/4} (f_{gas} \phi_P \alpha_{vir})^{3/8} \left( \frac{m_{*f}}{30M_\odot} \right)^{3/4} \Sigma_{cl}^{3/4} \left( \frac{m_*}{m_{*f}} \right)^{1/2} M_\odot \text{ yr}^{-1} \\ &\sim 4.6 \times 10^{-4} \left( \frac{m_{*f}}{30M_\odot} \right)^{3/4} \Sigma_{cl}^{3/4} \left( \frac{m_*}{m_{*f}} \right)^{1/2} M_\odot \text{ yr}^{-1} \end{aligned} \quad (2)$$

where  $\epsilon_{core}$  is the fraction of the total core mass ( $M_{core}$ ),  $\phi_P$  is the ratio of the core's surface pressure to the mean pressure in the clumps,  $f_{gas}$  is the fraction of the cloud's mass that is in gas, as opposed to stars,  $\Sigma_{cl}$  is a mean mass column density,  $m_*$  ( $=\epsilon_{core}M_{core}$ , where  $M_{core}$  is the total core mass) is the instantaneous mass (the current mass), and  $m_{*f}$  is the final mass of the star. We used the values of  $\Sigma_{cl} = 1$ ,  $\epsilon_{core} = 0.5$  and  $\phi_P = 0.663$  (see McKee & Tan (2002) for details). The bolometric luminosity is the sum of the internal and accretion luminosity ( $L_{bol} = L_{int} + L_{acc}$ ). The accretion luminosity is given by McKee & Tan (2003):

$$L_{acc} \sim 3.0 \times 10^4 \left( \frac{f_{acc}}{0.5} \right) \left( \frac{m_{*f}}{30M_\odot} \right)^{1.2} \Sigma_{cl}^{3/4} \left( \frac{m_*}{m_{*f}} \right)^{0.95} \Sigma_{cl}^{3/4} L_\odot \quad (3)$$

where  $f_{acc}$  ( $\ll 1$ ) is a factor that accounts for the energy advected into the star or used to drive protostellar outflows.

The internal luminosity,  $L_{int}$ , is equal to the luminosity transported by radiation and is determined mostly by the stellar mass ( $L_{int} \propto M_*^{5.5} R_*^{-0.5} \propto M_*$ ). A simple formula cannot be used for a wide range of masses of stars, because as the mass increases, the relative contribution of the Kramers and electron scattering opacities changes (Nakano et al. 2000). Therefore, in order to estimate the mass of star from the bolometric luminosity, we directly used Figure 2 of McKee



& Tan (2002). The instantaneous masses of TC3A and TC4A are 3-8  $M_{\odot}$  and 2-5  $M_{\odot}$  for the bolometric luminosities of  $\sim 1700$  and  $1200 L_{\odot}$ , respectively, assuming a significant amount of the 1.3mm flux is from Component A. The accreting properties of the TC3 core are similar to those of G34.24+0.1 (McKee & Tan 2003). We estimated accretion rates using the equation 2 for a grid of final masses of 7.5, 30 and 120  $M_{\odot}$ . The accretion rates for TC3 and TC4 are  $1-5 \times 10^{-4} M_{\odot} \text{ yr}^{-1}$  and  $0.9-4 \times 10^{-4} M_{\odot} \text{ yr}^{-1}$ , respectively. We also estimated the current masses and the accretion rates of TC1 and TC2 using  $L_{bol}$  of 600  $L_{\odot}$ ; the current masses are 1-3  $M_{\odot}$  and the accretion rates are  $0.8-1.7 \times 10^{-4} M_{\odot} \text{ yr}^{-1}$ . The estimated accretion luminosities infer that high portions of the bolometric luminosities are from accretion luminosities in the early stage of massive-star formation. The timescale of the infalling stage is determined mainly by the conditions in the stars' natal cloud and weakly depends on the mass of stars.

In the study of massive-star formation, a fundamental open question is how clusters are formed. Do massive dense cores have internal substructures? Do clumps evolve independently to produce stars, or do they share a common evolutionary process? Are apparent-single stars born single, or are they born in groups and subsequently ejected? While low-mass stars are believed to be produced mainly through accretion (Lada 1991), there are two main scenarios to explain high-mass star formation. One scenario is through accretion, like that of low-mass stars but with higher accretion rates; the other scenario is through formation of high-mass stars through coalescence of lower-mass protostars. We found 5 protostars for each of TC3 and TC4 cores, and the brightest and the most massive star in each cluster is located in the dust continuum peak (see Table 2), implying these systems are possible protoclusters. The brightest protostar appears near the center of the dust continuum peak. The brightest  $24\mu\text{m}$  source in the TC3, TC3A, is located in the millimeter peak and at the center of the core. Within the cluster, as the separation of TC3B-TC3C from the largest star of each Component A increases, the mid-infrared luminosity decreases in the case of the TC3 core, as shown in Table 2. This suggests that the brightest and most massive star among 4 protostars is located at the bottom of the gravitational potential well and is located where it formed, although the mid-infrared luminosities may not be directly correlated with the total bolometric luminosities. Accretion from gas or nearby fragmented clumps is found through the accretion of residual gas onto relatively low-mass cores. This picture may be consistent with the mass segregation, in young stellar clusters, and competitive accretion proposed by Bonnell & Davies (1998) and Bonnell et al. (2004). However, the brightest  $24\mu\text{m}$  source in the TC4 core, TC4A, is slightly off from the center of the millimeter peak, although TC4A is still the largest star in the cluster and the closest star to the dust continuum peak. The mid-infrared luminosity of TC4B is also smaller than that of the TC4A. It is unknown how these mid-infrared luminosities correlate with the total bolometric luminosities for individual sources. Comparable resolution far-infrared or millimeter observations are required in order to answer this question. Unfortunately, even through the Trifid Nebula is one of the nearest massive-star-forming regions with a distance of only 1.68 kpc, protostars in the Trifid as well as other comparable massive-star-forming regions are not bright enough for such observatories as the submillimeter Array (SMA). Future far-infrared observations with comparable spatial resolution are needed to answer this question.

We thank those who have been involved in the successful *Spitzer* mission and SSC colleagues who participated in the initial Early Release proposal of M 20. We thank Tom Jarrett for help in analyzing the Palomar/WIRC data. J. Rho thanks Susana Lizano for helpful discussion of early protostars. We thank Robert Hurt for producing Figures 1 and 5 for our press release. This work is based on observations made with the *Spitzer Space Telescope*, which is operated by the Jet Propulsion Laboratory, California Institute of Technology, under NASA contract 1407. Support for this work was provided by NASA through an award issued by JPL/Caltech.

Table 1. Protostars and Young Stellar Objects in the Trifid Nebula identified by the *Spitzer* color-color diagram

Class No.	SSTM20 (J2000)	MIPS 24 (mag)	IRAC 8 (mag)	IRAC 5.8 (mag)	IRAC 4.5 (mag)	IRAC 3.6 (mag)	K <sup>a</sup> (mag)	H <sup>a</sup> (mag)	J <sup>a</sup> (mag)
ClassI0 1	18:01:53.69-23:09:54.4	1.83± 0.01	5.49± 0.01	7.08± 0.01	9.74± 0.03	10.46± 0.03	14.71± 0.03	17.10± 0.12	99.99± 9.99
ClassI0 2	18:01:55.11-22:56:38.4	5.11± 0.05	8.36± 0.03	9.37± 0.04	10.21± 0.04	10.92± 0.04	14.26± 0.02	16.66± 0.12	99.99± 9.99
ClassI0 3	18:01:57.72-22:55:12.0	4.07± 0.03	8.08± 0.03	9.01± 0.03	10.48± 0.04	11.62± 0.12	17.11± 0.17	99.99± 9.99	99.99± 9.99
ClassI0 4	18:02:01.77-23:05:53.9	3.03± 0.02	7.13± 0.02	7.71± 0.01	99.99± 9.99	9.54± 0.02	12.91± 0.02	15.73± 0.05	19.09± 0.18
ClassI0 5	18:02:04.68-23:00:15.5	2.77± 0.09	7.34± 0.04	8.60± 0.03	10.04± 0.03	10.21± 0.03	12.03± 0.02	99.99± 9.99	99.99± 9.99
ClassI0 6	18:02:05.45-23:05:05.3	4.36± 0.10	7.92± 0.12	8.71± 0.05	9.57± 0.02	11.34± 0.05	16.49± 0.08	99.99± 9.99	99.99± 9.99
ClassI0 7	18:02:05.57-23:05:29.0	2.93± 0.03	7.88± 0.08	8.45± 0.03	9.66± 0.02	11.18± 0.04	99.99± 9.99	18.04± 0.40	99.99± 9.99
ClassI0 8	18:02:07.20-23:05:36.2	3.94± 0.08	7.18± 0.07	7.54± 0.03	8.30± 0.01	9.44± 0.02	14.43± 0.02	99.99± 9.99	99.99± 9.99
ClassI0 9	18:02:08.35-22:44:55.0	2.46± 0.03	6.80± 0.01	8.34± 0.02	10.29± 0.06	10.73± 0.04	99.99± 9.99	99.99± 9.99	99.99± 9.99
ClassI0 10	18:02:09.46-22:47:14.6	3.98± 0.06	7.17± 0.03	7.80± 0.02	8.65± 0.01	9.92± 0.02	99.99± 9.99	99.99± 9.99	99.99± 9.99
ClassI0 11	18:02:12.69-22:46:07.0	5.12± 0.22	9.62± 0.13	10.11± 0.08	10.85± 0.06	11.55± 0.09	99.99± 9.99	99.99± 9.99	99.99± 9.99
ClassI0 12	18:02:12.77-23:05:46.7	1.83± 0.02	5.92± 0.01	6.77± 0.01	8.25± 0.01	9.87± 0.02	14.23± 0.02	15.61± 0.06	17.17± 0.04
ClassI0 13	18:02:13.08-23:06:07.2	3.89± 0.11	8.59± 0.10	9.19± 0.04	9.75± 0.03	11.12± 0.04	15.46± 0.05	99.99± 9.99	99.99± 9.99
ClassI0 14	18:02:14.04-23:06:40.7	3.47± 0.09	8.16± 0.11	8.74± 0.06	10.15± 0.04	11.69± 0.08	16.71± 0.15	99.99± 9.99	19.53± 0.31
ClassI0 15	18:02:15.79-23:06:42.8	3.57± 0.10	7.51± 0.06	7.47± 0.01	8.26± 0.01	9.45± 0.02	15.06± 0.02	18.12± 0.44	99.99± 9.99
ClassI0 16	18:02:16.80-23:03:47.2	1.94± 0.08	7.61± 0.04	8.91± 0.04	9.58± 0.03	10.53± 0.04	11.93± 0.02	12.26± 0.02	12.99± 0.02
ClassI0 17	18:02:16.85-23:00:51.8	1.13± 0.06	5.39± 0.02	6.12± 0.01	7.25± 0.01	8.38± 0.01	14.61± 0.02	17.53± 0.21	99.99± 9.99
ClassI0 18	18:02:22.92-22:55:41.2	0.81± 0.01	3.57± 0.00	4.45± 0.00	6.02± 0.00	7.32± 0.01	12.44± 0.02	14.81± 0.04	15.62± 0.02
ClassI0 19	18:02:24.68-23:01:17.7	2.02± 0.90	8.87± 0.55	9.19± 0.17	9.70± 0.06	10.68± 0.11	17.24± 0.35	17.91± 0.29	19.43± 0.27
ClassI0 20	18:02:25.25-22:46:04.4	3.05± 0.04	7.78± 0.06	8.61± 0.03	9.41± 0.02	10.21± 0.03	13.68± 0.02	15.86± 0.08	17.98± 0.08
ClassI0 21	18:02:25.90-22:46:00.1	2.34± 0.02	7.10± 0.03	9.00± 0.05	99.99± 9.99	11.51± 0.08	13.59± 0.02	14.52± 0.02	16.18± 0.02
ClassI0 22	18:02:25.99-22:45:51.1	2.53± 0.03	6.30± 0.01	7.25± 0.01	7.96± 0.01	8.66± 0.01	11.23± 0.02	13.25± 0.02	16.11± 0.02
ClassI0 23	18:02:27.26-23:03:20.5	1.75± 0.08	5.74± 0.01	6.35± 0.01	7.45± 0.01	8.86± 0.02	11.78± 0.02	15.27± 0.04	99.99± 9.99
ClassI0 24	18:02:28.49-23:03:56.9	2.09± 0.11	5.76± 0.02	7.69± 0.03	10.48± 0.06	10.78± 0.07	13.57± 0.02	16.20± 0.08	19.15± 0.20
ClassI0 25	18:02:30.34-23:00:22.7	1.82± 0.04	7.46± 0.13	8.40± 0.07	9.56± 0.03	10.80± 0.06	16.17± 0.03	17.58± 0.27	99.99± 9.99
ClassI0 26	18:02:31.71-22:56:47.0	1.58± 0.01	4.80± 0.01	5.45± 0.00	6.29± 0.00	6.92± 0.01	9.07± 0.02	11.34± 0.02	15.40± 0.02
ClassI0 27	18:02:34.04-23:06:56.9	5.16± 0.50	8.07± 0.09	8.71± 0.04	9.48± 0.02	10.10± 0.04	12.69± 0.02	14.41± 0.03	18.15± 0.10
ClassI0 28	18:02:34.17-23:06:53.3	5.16± 0.50	8.04± 0.08	8.70± 0.04	9.53± 0.02	10.06± 0.03	11.16± 0.02	12.85± 0.02	16.47± 0.02
ClassI0 29	18:02:34.46-23:08:06.4	1.99± 0.01	4.73± 0.01	5.23± 0.00	6.07± 0.00	6.64± 0.00	9.66± 0.02	12.38± 0.02	16.98± 0.03
ClassI0 30	18:02:34.85-22:49:55.2	2.07± 0.04	5.86± 0.03	6.68± 0.01	7.79± 0.01	8.74± 0.01	12.53± 0.02	16.24± 0.10	18.78± 0.13
ClassI0 31	18:02:40.73-23:00:30.6	1.75± 0.01	5.39± 0.02	6.01± 0.01	6.88± 0.01	7.42± 0.01	9.60± 0.02	12.13± 0.02	16.88± 0.04
ClassI0 32	18:02:41.30-22:44:38.4	1.69± 0.03	5.84± 0.03	7.63± 0.03	99.99± 9.99	11.52± 0.16	14.02± 0.02	14.88± 0.03	16.31± 0.02
ClassI0 33	18:02:42.41-22:44:12.8	0.50± 0.01	3.97± 0.00	5.77± 0.01	8.75± 0.03	8.97± 0.03	14.05± 0.05	14.78± 0.05	16.26± 0.04
ClassI0 34	18:02:42.41-22:44:12.8	0.50± 0.01	3.97± 0.00	5.77± 0.01	8.75± 0.03	8.97± 0.03	14.05± 0.05	14.78± 0.05	16.26± 0.04

Table 1—Continued

Class No.	SSTM20 (J2000)	MIPS 24 (mag)	IRAC 8 (mag)	IRAC 5.8 (mag)	IRAC 4.5 (mag)	IRAC 3.6 (mag)	K <sup>a</sup> (mag)	H <sup>a</sup> (mag)	J <sup>a</sup> (mag)
ClassI0 35	18:02:47.26-23:06:13.0	3.58± 0.09	7.44± 0.08	8.89± 0.07	10.15± 0.03	10.31± 0.03	12.98± 0.02	14.40± 0.02	16.28± 0.02
ClassI0 36	18:02:56.33-22:43:58.1	5.32± 0.18	8.15± 0.05	9.11± 0.04	10.66± 0.05	10.69± 0.05	99.99± 9.99	99.99± 9.99	99.99± 9.99
ClassI0 37	18:02:56.78-22:50:31.6	3.80± 0.05	7.25± 0.02	8.10± 0.02	9.04± 0.02	10.11± 0.04	99.99± 9.99	99.99± 9.99	99.99± 9.99
Hotex 1	18:01:53.42-22:51:55.4	2.76± 0.01	4.54± 0.00	5.19± 0.00	6.37± 0.00	8.09± 0.01	12.23± 0.02	99.99± 9.99	99.99± 9.99
Hotex 2	18:01:59.33-22:52:36.1	1.10± 0.01	3.66± 0.00	4.28± 0.00	5.56± 0.00	6.32± 0.00	8.34± 0.02	10.56± 0.02	14.85± 0.02
Hotex 3	18:01:59.36-23:07:38.6	1.15± 0.00	3.62± 0.00	4.25± 0.00	5.57± 0.00	6.75± 0.01	9.62± 0.02	12.29± 0.02	99.99± 9.99
Hotex 4	18:02:04.85-23:07:19.2	1.35± 0.01	3.56± 0.00	3.85± 0.00	5.33± 0.00	6.14± 0.00	10.52± 0.02	17.00± 0.19	99.99± 9.99
Hotex 5	18:02:05.52-23:06:51.1	1.50± 0.01	4.03± 0.00	4.24± 0.00	5.55± 0.00	6.09± 0.00	8.34± 0.02	12.08± 0.02	99.99± 9.99
Hotex 6	18:02:05.52-23:04:39.4	7.34± 0.59	9.59± 0.01	9.49± 0.05	10.10± 0.03	11.57± 0.05	99.99 ± 9.99	20.07± 0.78	20.11± 0.42
Hotex 7	18:02:08.95-22:45:29.5	1.45± 0.01	4.07± 0.00	4.96± 0.00	99.99± 9.99	6.99± 0.01	99.99± 9.99	99.99± 9.99	99.99± 9.99
Hotex 8	18:02:12.48-23:05:16.1	4.88± 0.28	6.74± 0.01	7.48± 0.01	8.37± 0.01	9.18± 0.02	12.03± 0.02	13.91± 0.02	16.28± 0.02
Hotex 9	18:02:12.50-23:05:15.4	4.88± 0.28	6.75± 0.01	7.47± 0.01	8.37± 0.01	9.18± 0.02	12.03± 0.02	13.91± 0.02	16.28± 0.02
Hotex 10	18:02:17.64-22:56:54.2	1.74± 0.02	3.86± 0.00	4.32± 0.00	5.45± 0.00	6.13± 0.01	8.32± 0.02	9.79± 0.02	13.31± 0.02
Hotex 11	18:02:22.75-23:09:30.6	1.65± 0.01	4.06± 0.00	4.48± 0.00	5.72± 0.00	6.20± 0.00	8.22± 0.02	10.27± 0.02	14.69± 0.02
Hotex 12	18:02:49.70-22:49:05.5	3.25± 0.02	4.80± 0.00	5.11± 0.00	6.00± 0.00	6.80± 0.01	9.21± 0.02	10.45± 0.02	13.17± 0.02
Hotex 13	18:02:50.79-23:11:29.8	2.60± 0.01	4.40± 0.00	5.29± 0.00	6.09± 0.00	7.75± 0.01	11.68± 0.02	15.64± 0.08	99.99± 9.99
ClassII 1	18:01:51.67-22:49:49.8	3.19± 0.01	5.29± 0.01	5.65± 0.00	6.06± 0.00	6.51± 0.00	99.99± 9.99	99.99± 9.99	99.99± 9.99
ClassII 2	18:01:52.18-22:52:45.8	3.51± 0.03	6.55± 0.01	6.62± 0.01	6.80± 0.01	6.88± 0.01	8.38± 0.02	9.52± 0.02	99.99± 9.99
ClassII 3	18:01:52.54-22:50:06.4	2.78± 0.01	4.85± 0.00	5.17± 0.00	5.78± 0.00	6.42± 0.00	99.99± 9.99	99.99± 9.99	99.99± 9.99
ClassII 4	18:01:53.81-23:03:34.9	4.57± 0.03	8.62± 0.05	8.96± 0.03	99.99± 9.99	9.57± 0.02	11.67± 0.02	13.09± 0.02	14.99± 0.02
ClassII 5	18:01:54.05-23:11:51.7	3.91± 0.04	7.44± 0.02	8.31± 0.02	8.32± 0.01	8.96± 0.01	11.82± 0.02	15.12± 0.04	21.13± 0.75
ClassII 6	18:01:54.46-23:05:51.7	4.67± 0.05	7.24± 0.01	7.27± 0.01	99.99± 9.99	7.85± 0.01	9.67± 0.02	12.02± 0.02	16.67± 0.03
ClassII 7	18:01:54.55-22:53:58.6	3.27± 0.03	6.36± 0.01	6.39± 0.01	6.82± 0.01	6.87± 0.01	8.43± 0.02	9.86± 0.02	13.07± 0.02
ClassII 8	18:01:55.06-22:49:45.5	4.36± 0.05	7.52± 0.03	7.55± 0.01	8.01± 0.01	8.15± 0.01	99.99± 9.99	99.99± 9.99	99.99± 9.99
ClassII 9	18:01:55.34-22:46:43.7	3.82± 0.02	6.55± 0.01	7.07± 0.01	7.58± 0.01	7.99± 0.01	99.99± 9.99	99.99± 9.99	99.99± 9.99
ClassII 10	18:01:55.73-22:55:16.7	3.77± 0.04	6.03± 0.01	6.15± 0.01	6.43± 0.00	6.68± 0.01	8.35± 0.02	9.89± 0.02	13.37± 0.02
ClassII 11	18:01:58.08-22:51:31.7	4.44± 0.09	6.75± 0.01	6.84± 0.01	7.35± 0.01	7.25± 0.01	99.99± 9.99	99.99± 9.99	99.99± 9.99
ClassII 12	18:01:58.61-22:44:49.6	4.92± 0.08	7.47± 0.04	7.33± 0.02	99.99± 9.99	7.45± 0.01	99.99± 9.99	99.99± 9.99	99.99± 9.99
ClassII 13	18:01:58.63-23:01:35.0	5.06± 0.29	7.39± 0.03	7.44± 0.01	7.85± 0.01	8.07± 0.01	9.79± 0.02	11.40± 0.02	14.83± 0.02
ClassII 14	18:01:58.65-23:06:19.8	4.58± 0.08	8.32± 0.04	8.29± 0.02	8.69± 0.01	8.71± 0.01	10.34± 0.02	12.53± 0.02	16.86± 0.03
ClassII 15	18:01:58.97-23:08:23.6	4.52± 0.05	6.82± 0.02	6.76± 0.01	7.19± 0.01	7.33± 0.01	9.08± 0.02	11.29± 0.02	15.72± 0.02
ClassII 16	18:01:59.38-23:03:07.6	3.37± 0.05	6.37± 0.01	6.65± 0.01	7.06± 0.01	7.58± 0.01	10.17± 0.02	12.77± 0.02	99.99± 9.99
ClassII 17	18:01:59.38-22:48:12.6	4.92± 0.05	8.05± 0.04	7.97± 0.02	8.41± 0.01	8.56± 0.01	99.99± 9.99	99.99± 9.99	99.99± 9.99
ClassII 18	18:01:59.40-23:05:56.8	4.23± 0.05	6.28± 0.01	6.38± 0.01	6.78± 0.01	7.14± 0.01	8.97± 0.02	11.21± 0.02	15.60± 0.02

Table 1—Continued

Class No.	SSTM20 (J2000)	MIPS 24 (mag)	IRAC 8 (mag)	IRAC 5.8 (mag)	IRAC 4.5 (mag)	IRAC 3.6 (mag)	K <sup>a</sup> (mag)	H <sup>a</sup> (mag)	J <sup>a</sup> (mag)
ClassII 19	18:02:01.56-23:01:11.3	5.18± 0.38	8.12± 0.07	8.13± 0.02	8.41± 0.01	8.78± 0.01	10.22± 0.02	12.32± 0.02	16.52± 0.02
ClassII 20	18:02:02.31-22:49:12.7	4.47± 0.05	8.67± 0.04	8.65± 0.02	9.16± 0.02	9.20± 0.02	99.99± 9.99	99.99± 9.99	99.99± 9.99
ClassII 21	18:02:03.19-22:48:48.6	1.75± 0.01	5.07± 0.00	5.69± 0.00	6.26± 0.00	6.60± 0.00	99.99± 9.99	99.99± 9.99	99.99± 9.99
ClassII 22	18:02:05.62-22:46:39.7	4.91± 0.10	7.70± 0.03	7.60± 0.01	8.06± 0.01	8.04± 0.01	99.99± 9.99	99.99± 9.99	99.99± 9.99
ClassII 23	18:02:05.86-22:47:41.6	5.25± 0.20	8.13± 0.03	8.08± 0.02	8.49± 0.01	8.85± 0.01	99.99± 9.99	99.99± 9.99	99.99± 9.99
ClassII 24	18:02:07.15-22:49:07.0	2.72± 0.02	6.96± 0.02	6.96± 0.01	7.28± 0.01	7.41± 0.01	99.99± 9.99	99.99± 9.99	99.99± 9.99
ClassII 25	18:02:08.38-22:49:04.4	3.70± 0.03	7.00± 0.01	7.15± 0.01	7.75± 0.01	7.92± 0.01	99.99± 9.99	99.99± 9.99	99.99± 9.99
ClassII 26	18:02:08.59-22:48:59.0	3.70± 0.03	6.55± 0.01	6.66± 0.01	6.72± 0.01	6.78± 0.01	99.99± 9.99	99.99± 9.99	99.99± 9.99
ClassII 27	18:02:09.60-22:49:28.9	4.20± 0.14	7.39± 0.02	7.29± 0.01	7.82± 0.01	7.63± 0.01	99.99± 9.99	99.99± 9.99	99.99± 9.99
ClassII 28	18:02:09.74-22:56:01.3	2.60± 0.03	5.61± 0.01	5.79± 0.01	6.24± 0.00	6.71± 0.00	8.36± 0.02	10.27± 0.02	14.54± 0.02
ClassII 29	18:02:10.30-22:54:55.8	4.36± 0.14	7.30± 0.03	7.75± 0.02	8.37± 0.01	8.73± 0.01	11.25± 0.02	16.47± 0.02	99.99± 9.99
ClassII 30	18:02:10.94-22:47:56.8	4.67± 0.16	7.76± 0.04	7.79± 0.02	8.20± 0.01	8.40± 0.01	99.99± 9.99	99.99± 9.99	99.99± 9.99
ClassII 31	18:02:11.71-22:47:42.4	5.68± 0.45	9.06± 0.09	9.78± 0.07	10.34± 0.04	10.68± 0.04	99.99± 9.99	99.99± 9.99	99.99± 9.99
ClassII 32	18:02:12.67-22:58:52.7	2.87± 0.08	6.16± 0.02	6.19± 0.01	6.50± 0.00	6.60± 0.00	8.22± 0.02	9.70± 0.02	13.18± 0.02
ClassII 33	18:02:12.89-22:54:40.7	4.62± 0.17	6.80± 0.02	6.85± 0.01	7.00± 0.01	6.92± 0.01	7.93± 0.02	8.76± 0.02	10.54± 0.02
ClassII 34	18:02:12.99-22:49:45.5	4.70± 0.09	7.74± 0.03	7.82± 0.02	7.96± 0.01	7.84± 0.01	99.99± 9.99	99.99± 9.99	99.99± 9.99
ClassII 35	18:02:14.21-23:01:44.0	0.75± 0.04	3.93± 0.00	5.26± 0.00	5.82± 0.00	6.57± 0.00	8.74± 0.02	10.21± 0.02	11.99± 0.02
ClassII 36	18:02:14.33-22:45:57.2	4.18± 0.05	7.27± 0.02	7.24± 0.01	7.66± 0.01	7.80± 0.01	99.99± 9.99	99.99± 9.99	99.99± 9.99
ClassII 37	18:02:15.86-23:05:55.7	3.68± 0.14	7.64± 0.05	9.32± 0.06	10.15± 0.04	10.47± 0.03	11.72± 0.02	12.33± 0.02	13.39± 0.02
ClassII 38	18:02:16.22-22:48:33.1	4.28± 0.07	6.48± 0.01	6.54± 0.01	6.76± 0.01	7.05± 0.01	8.41± 0.02	9.53± 0.02	99.99± 9.99
ClassII 39	18:02:16.77-22:54:37.4	3.75± 0.08	6.33± 0.01	6.38± 0.01	6.71± 0.01	6.94± 0.01	8.75± 0.02	11.28± 0.02	16.23± 0.02
ClassII 40	18:02:16.97-23:09:46.8	4.81± 0.06	7.45± 0.03	7.37± 0.01	7.77± 0.01	7.90± 0.01	9.40± 0.02	11.38± 0.02	15.35± 0.02
ClassII 41	18:02:17.69-23:07:17.0	4.32± 0.25	8.06± 0.10	8.07± 0.03	8.76± 0.02	9.12± 0.02	12.33± 0.02	16.20± 0.11	99.99± 9.99
ClassII 42	18:02:18.19-23:07:50.5	3.68± 0.03	6.48± 0.04	6.74± 0.02	7.27± 0.01	7.64± 0.01	9.99± 0.02	12.44± 0.02	17.29± 0.04
ClassII 43	18:02:18.60-22:49:48.0	4.25± 0.07	6.85± 0.01	6.89± 0.01	7.23± 0.01	7.22± 0.01	8.91± 0.02	10.84± 0.02	99.99± 9.99
ClassII 44	18:02:19.25-22:55:13.1	3.66± 0.02	8.31± 0.10	9.37± 0.09	9.90± 0.03	9.86± 0.03	10.71± 0.02	11.84± 0.02	14.23± 0.02
ClassII 45	18:02:21.91-22:47:53.5	5.44± 0.10	7.79± 0.03	7.81± 0.02	8.27± 0.01	8.20± 0.01	9.58± 0.02	11.25± 0.02	14.56± 0.02
ClassII 46	18:02:23.23-23:01:35.0	2.65± 0.30	6.17± 0.06	6.56± 0.03	6.96± 0.01	7.34± 0.01	8.86± 0.02	9.95± 0.02	11.31± 0.02
ClassII 47	18:02:25.37-23:06:15.8	2.57± 0.09	5.70± 0.01	5.99± 0.01	6.66± 0.01	7.04± 0.01	9.25± 0.02	12.15± 0.02	17.38± 0.04
ClassII 48	18:02:25.47-22:50:19.7	6.01± 0.44	8.03± 0.03	7.99± 0.01	8.26± 0.01	8.19± 0.01	9.32± 0.02	10.77± 0.02	13.72± 0.02
ClassII 49	18:02:26.93-22:50:37.3	3.66± 0.03	6.19± 0.01	6.32± 0.01	6.67± 0.01	6.90± 0.01	8.24± 0.02	9.48± 0.02	11.95± 0.02
ClassII 50	18:02:30.67-22:58:01.2	3.18± 0.05	6.13± 0.03	6.19± 0.01	6.65± 0.01	6.98± 0.01	8.42± 0.02	10.04± 0.02	13.79± 0.02
ClassII 51	18:02:30.96-23:02:35.2	2.91± 0.14	7.86± 0.07	8.88± 0.04	9.41± 0.02	9.64± 0.02	10.91± 0.02	11.56± 0.02	12.15± 0.02
ClassII 52	18:02:31.77-22:57:53.6	3.54± 0.14	6.07± 0.03	6.51± 0.01	6.62± 0.01	6.61± 0.00	7.89± 0.02	8.71± 0.02	10.61± 0.02

Table 1—Continued

Class No.	SSTM20 (J2000)	MIPS 24 (mag)	IRAC 8 (mag)	IRAC 5.8 (mag)	IRAC 4.5 (mag)	IRAC 3.6 (mag)	K <sup>a</sup> (mag)	H <sup>a</sup> (mag)	J <sup>a</sup> (mag)
ClassII 53	18:02:32.76-22:49:00.5	5.41± 0.16	7.64± 0.02	7.72± 0.01	8.06± 0.01	7.89± 0.01	9.32± 0.02	10.64± 0.02	12.06± 0.02
ClassII 54	18:02:32.97-22:53:49.2	4.10± 0.04	6.59± 0.02	6.71± 0.01	7.00± 0.01	7.06± 0.01	8.52± 0.02	9.95± 0.02	13.23± 0.02
ClassII 55	18:02:33.27-23:02:23.6	2.12± 0.08	5.55± 0.01	5.57± 0.00	6.03± 0.00	6.43± 0.00	8.29± 0.02	9.95± 0.02	13.85± 0.02
ClassII 56	18:02:33.65-23:09:02.9	3.71± 0.02	7.32± 0.03	7.37± 0.01	7.94± 0.01	7.83± 0.01	9.41± 0.02	11.41± 0.02	15.36± 0.02
ClassII 57	18:02:33.65-23:09:02.9	3.71± 0.02	7.32± 0.03	7.37± 0.01	7.94± 0.01	7.83± 0.01	9.41± 0.02	11.41± 0.02	15.36± 0.02
ClassII 58	18:02:33.82-22:53:26.9	4.19± 0.04	6.83± 0.01	6.84± 0.01	7.23± 0.01	7.18± 0.01	8.78± 0.02	10.53± 0.02	99.99± 9.99
ClassII 59	18:02:34.44-22:59:16.4	4.17± 0.22	6.68± 0.02	7.30± 0.01	7.99± 0.01	8.42± 0.01	10.59± 0.02	12.46± 0.02	16.15± 0.02
ClassII 60	18:02:35.04-22:58:22.4	2.99± 0.06	5.30± 0.01	5.33± 0.00	5.91± 0.00	6.02± 0.00	7.84± 0.02	8.61± 0.02	10.52± 0.02
ClassII 61	18:02:35.23-22:58:10.6	2.95± 0.07	7.54± 0.10	8.28± 0.05	9.14± 0.02	9.11± 0.03	10.65± 0.02	12.52± 0.02	16.46± 0.03
ClassII 62	18:02:36.17-23:09:14.4	4.83± 0.10	7.69± 0.04	7.73± 0.01	8.15± 0.01	8.26± 0.01	9.82± 0.02	11.93± 0.02	16.17± 0.02
ClassII 63	18:02:36.50-22:44:08.5	5.05± 0.32	8.16± 0.03	8.08± 0.02	99.99± 9.99	8.32± 0.01	9.29± 0.02	10.62± 0.02	13.59± 0.02
ClassII 64	18:02:37.35-22:48:57.2	3.77± 0.05	7.39± 0.03	7.57± 0.01	7.88± 0.01	7.70± 0.01	9.13± 0.02	10.47± 0.02	13.31± 0.02
ClassII 65	18:02:37.65-22:46:59.5	3.42± 0.03	6.49± 0.02	6.99± 0.01	7.25± 0.01	7.39± 0.01	8.55± 0.02	9.77± 0.02	12.58± 0.02
ClassII 66	18:02:38.95-22:58:41.9	3.73± 0.09	7.11± 0.05	7.29± 0.01	7.79± 0.01	8.16± 0.01	9.74± 0.02	11.88± 0.02	99.99± 9.99
ClassII 67	18:02:40.03-23:05:55.7	3.52± 0.08	7.06± 0.07	7.02± 0.02	7.42± 0.01	7.51± 0.01	8.89± 0.02	10.41± 0.02	13.66± 0.02
ClassII 68	18:02:40.42-23:08:50.6	4.93± 0.08	7.05± 0.03	7.35± 0.01	7.57± 0.01	7.84± 0.01	9.44± 0.02	11.02± 0.02	14.49± 0.02
ClassII 69	18:02:41.07-23:08:43.4	4.78± 0.07	6.91± 0.02	7.28± 0.01	7.58± 0.01	7.73± 0.01	8.97± 0.02	10.50± 0.02	13.83± 0.02
ClassII 70	18:02:41.45-22:51:42.1	3.07± 0.02	7.69± 0.07	7.76± 0.02	8.07± 0.01	8.23± 0.01	9.81± 0.02	11.78± 0.02	99.99± 9.99
ClassII 71	18:02:41.64-23:00:03.6	2.95± 0.05	6.46± 0.03	6.65± 0.01	7.14± 0.01	7.39± 0.01	9.91± 0.02	12.06± 0.02	16.73± 0.03
ClassII 72	18:02:42.17-23:02:39.1	3.00± 0.06	6.97± 0.05	7.56± 0.02	8.09± 0.01	8.33± 0.01	10.12± 0.02	12.26± 0.02	15.99± 0.02
ClassII 73	18:02:42.99-23:03:13.0	3.63± 0.14	7.53± 0.04	8.99± 0.05	10.15± 0.03	10.27± 0.04	11.37± 0.02	12.06± 0.02	13.26± 0.02
ClassII 74	18:02:43.10-23:07:21.4	3.72± 0.06	8.51± 0.10	8.53± 0.03	8.96± 0.02	9.02± 0.01	10.56± 0.02	12.70± 0.02	16.82± 0.03
ClassII 75	18:02:43.82-23:05:30.1	4.63± 0.18	6.92± 0.02	7.02± 0.01	7.48± 0.01	7.13± 0.01	8.51± 0.02	9.88± 0.02	12.72± 0.02
ClassII 76	18:02:45.00-23:08:05.3	4.29± 0.06	7.49± 0.03	7.52± 0.01	7.97± 0.01	7.86± 0.01	9.48± 0.02	11.28± 0.02	14.83± 0.02
ClassII 77	18:02:45.07-23:03:17.3	4.36± 0.20	7.70± 0.05	7.86± 0.02	8.23± 0.01	8.34± 0.01	9.77± 0.02	11.46± 0.02	15.06± 0.02
ClassII 78	18:02:45.38-22:48:51.8	3.39± 0.05	6.67± 0.01	6.59± 0.01	7.16± 0.01	7.36± 0.01	8.94± 0.02	10.72± 0.02	14.34± 0.02
ClassII 79	18:02:45.41-22:46:07.0	3.80± 0.05	7.29± 0.03	8.42± 0.04	9.17± 0.02	9.06± 0.02	9.16± 0.02	9.44± 0.02	10.62± 0.02
ClassII 80	18:02:45.81-22:44:22.9	3.00± 0.03	7.90± 0.09	7.94± 0.03	99.99± 9.99	8.05± 0.01	9.04± 0.02	10.35± 0.02	13.23± 0.02
ClassII 81	18:02:48.93-22:45:41.4	4.47± 0.14	7.22± 0.02	7.69± 0.01	99.99± 9.99	7.86± 0.01	9.82± 0.02	12.01± 0.02	16.21± 0.02
ClassII 82	18:02:49.20-22:59:45.6	4.18± 0.19	8.86± 0.15	9.99± 0.09	10.19± 0.03	10.46± 0.03	11.30± 0.02	12.02± 0.02	13.12± 0.02
ClassII 83	18:02:50.16-23:03:39.2	3.08± 0.03	5.17± 0.01	5.62± 0.00	6.23± 0.00	6.72± 0.01	8.71± 0.02	9.99± 0.02	12.97± 0.02
ClassII 84	18:02:50.45-22:48:50.0	4.75± 0.10	7.40± 0.02	7.30± 0.01	7.40± 0.01	7.38± 0.01	8.01± 0.02	8.89± 0.02	10.52± 0.02
ClassII 85	18:02:50.54-23:09:23.4	4.55± 0.03	7.55± 0.02	8.08± 0.01	8.59± 0.01	8.41± 0.01	9.47± 0.02	10.85± 0.02	13.65± 0.02
ClassII 86	18:02:51.53-22:46:41.5	4.80± 0.14	7.63± 0.03	7.62± 0.01	7.90± 0.01	7.81± 0.01	8.72± 0.02	99.99± 9.99	12.38± 0.02



Table 1—Continued

Class No.	SSTM20 (J2000)	MIPS 24 (mag)	IRAC 8 (mag)	IRAC 5.8 (mag)	IRAC 4.5 (mag)	IRAC 3.6 (mag)	K <sup>a</sup> (mag)	H <sup>a</sup> (mag)	J <sup>a</sup> (mag)
ClassII 87	18:02:51.62-22:47:50.6	4.61± 0.10	7.92± 0.04	8.41± 0.02	8.74± 0.01	8.59± 0.01	9.65± 0.02	99.99± 9.99	13.28± 0.02
ClassII 88	18:02:51.67-23:02:07.1	4.93± 0.16	7.70± 0.02	7.69± 0.01	8.02± 0.01	7.95± 0.01	9.00± 0.02	10.45± 0.02	13.51± 0.02
ClassII 89	18:02:51.69-23:05:13.6	4.74± 0.06	7.04± 0.02	7.23± 0.01	7.85± 0.01	7.73± 0.01	9.03± 0.02	10.39± 0.02	13.22± 0.02
ClassII 90	18:02:51.99-23:03:56.5	3.85± 0.06	8.58± 0.09	10.56± 0.16	10.59± 0.04	11.08± 0.07	12.43± 0.02	13.79± 0.02	16.49± 0.02
ClassII 91	18:02:52.39-23:00:42.1	3.73± 0.09	7.06± 0.03	7.04± 0.01	7.42± 0.01	7.51± 0.01	8.85± 0.02	10.65± 0.02	14.51± 0.02
ClassII 92	18:02:53.59-22:53:30.5	5.56± 0.07	7.87± 0.03	7.87± 0.01	8.10± 0.01	8.09± 0.01	8.92± 0.02	10.23± 0.02	12.94± 0.02
ClassII 93	18:02:53.61-22:45:32.0	4.72± 0.11	8.07± 0.04	8.26± 0.02	99.99± 9.99	8.47± 0.01	9.55± 0.02	99.99± 9.99	13.90± 0.02
ClassII 94	18:02:53.98-23:09:22.3	5.11± 0.07	7.25± 0.02	7.46± 0.01	7.59± 0.01	7.61± 0.01	8.68± 0.02	9.83± 0.02	12.34± 0.02
ClassII 95	18:02:55.42-22:46:34.3	4.30± 0.05	6.91± 0.02	7.16± 0.01	7.77± 0.01	8.06± 0.01	99.99± 9.99	99.99± 9.99	99.99± 9.99
ClassII 96	18:02:56.18-23:05:10.0	3.72± 0.05	6.92± 0.04	7.20± 0.01	7.54± 0.01	7.68± 0.01	8.87± 0.02	10.24± 0.02	13.23± 0.02
ClassII 97	18:02:57.29-22:46:11.6	5.46± 0.11	7.84± 0.05	7.79± 0.02	8.12± 0.01	8.29± 0.01	99.99± 9.99	99.99± 9.99	99.99± 9.99
ClassII 98	18:02:57.46-22:57:26.6	4.78± 0.04	8.82± 0.12	8.50± 0.03	8.73± 0.02	8.90± 0.01	10.31± 0.02	12.33± 0.02	16.22± 0.02
ClassII 99	18:02:57.55-22:47:29.0	5.33± 0.05	7.66± 0.02	7.74± 0.01	8.15± 0.01	7.99± 0.01	99.99± 9.99	99.99± 9.99	99.99± 9.99
ClassIII100	18:02:57.60-22:45:28.4	4.86± 0.08	7.85± 0.05	8.21± 0.02	99.99± 9.99	8.91± 0.02	99.99± 9.99	99.99± 9.99	99.99± 9.99
ClassIII101	18:02:58.03-22:51:57.6	4.49± 0.05	7.29± 0.02	7.33± 0.01	7.59± 0.01	7.44± 0.01	8.31± 0.02	9.18± 0.02	10.85± 0.02
ClassIII102	18:02:58.27-22:59:53.5	4.65± 0.07	6.92± 0.02	6.97± 0.01	7.09± 0.01	7.21± 0.01	8.02± 0.02	8.94± 0.02	10.64± 0.02
ClassIII103	18:03:00.17-23:00:34.2	5.39± 0.10	8.31± 0.03	8.58± 0.02	8.89± 0.02	8.93± 0.01	10.30± 0.02	11.91± 0.02	15.34± 0.02
ClassIII104	18:03:00.19-23:03:07.6	5.23± 0.15	7.45± 0.03	7.43± 0.01	7.69± 0.01	7.70± 0.01	8.73± 0.02	9.96± 0.02	12.63± 0.02
ClassIII105	18:03:01.20-23:03:35.3	3.82± 0.04	7.38± 0.03	7.58± 0.01	7.83± 0.01	7.83± 0.01	8.90± 0.02	10.27± 0.02	99.99± 9.99
ClassIII106	18:03:02.14-22:59:48.5	4.65± 0.07	6.97± 0.02	7.22± 0.01	7.62± 0.01	7.40± 0.01	8.25± 0.02	9.28± 0.02	11.07± 0.02
ClassIII107	18:03:02.76-22:58:52.0	3.76± 0.04	8.16± 0.14	7.93± 0.03	8.13± 0.01	8.22± 0.01	9.72± 0.02	99.99± 9.99	14.60± 0.02
ClassIII108	18:03:03.38-22:57:19.1	3.91± 0.03	7.94± 0.05	7.85± 0.02	8.27± 0.01	8.19± 0.01	9.24± 0.02	99.99± 9.99	13.57± 0.02
ClassIII109	18:03:03.50-22:57:03.6	4.23± 0.06	7.76± 0.05	8.25± 0.02	8.45± 0.01	8.76± 0.01	10.26± 0.02	99.99± 9.99	15.96± 0.02
ClassIII110	18:03:03.82-22:57:34.9	3.75± 0.02	7.11± 0.03	7.30± 0.01	7.74± 0.01	7.67± 0.01	8.85± 0.02	99.99± 9.99	13.56± 0.02
ClassIII111	18:03:04.27-23:08:02.4	4.97± 0.04	8.04± 0.02	9.41± 0.03	9.76± 0.03	10.07± 0.03	12.13± 0.02	99.99± 9.99	14.26± 0.02



Table 2. Properties of Protostars within the Four Dust Continuum Cores

name	(J2000)	(mag)	(mag)	(mag)	(mag)	(mag)	(mag)	(mag)	(mag)	(mag)	( $''$ )	( $L_{\odot}$ )
TC3A	18:02:05.57-23:05:29.0	2.93 0.03	7.88 0.08	8.45 0.03	9.66 0.02	11.18 0.04	99.99 9.99	18.04 0.40	99.99 9.99	99.99 9.99	0	13
TC3B	18:02:07.20-23:05:36.2	3.94 0.08	7.18 0.07	7.54 0.03	8.30 0.01	9.44 0.02	14.43 0.02	99.99 9.99	99.99 9.99	99.99 9.99	23.6	9
TC3C	18:02:05.45-23:05:05.3	4.36 0.10	7.92 0.12	8.71 0.05	9.57 0.02	11.34 0.05	16.49 0.08	99.99 9.99	99.99 9.99	99.99 9.99	23.8	4
TC3D	18:02:05.52-23:04:39.4	7.34 0.59	9.59 0.01	9.49 0.05	10.10 0.03	11.57 0.05	99.99 9.99	20.07 0.78	20.11 0.42	49.7	1	
TC3E	18:02:01.77-23:05:53.9	3.03 0.02	7.13 0.02	7.71 0.01	99.99 9.99	9.54 0.02	12.91 0.02	15.73 0.05	19.09 0.18	57.9	16	
TC4A	18:02:12.77-23:05:46.7	1.83 0.02	5.92 0.01	6.77 0.01	8.25 0.01	9.87 0.02	14.23 0.02	15.61 0.06	17.17 0.04	0	32	
TC4B	18:02:13.08-23:06:07.2	3.89 0.11	8.59 0.10	9.19 0.04	9.75 0.03	11.12 0.04	15.46 0.05	99.99 9.99	99.99 9.99	21.0	5	
TC4C	18:02:12.50-23:05:15.4	4.88 0.28	6.75 0.01	7.47 0.01	8.37 0.01	9.18 0.02	12.03 0.02	13.91 0.02	16.28 0.02	31.5	9	
TC4D	18:02:14.04-23:06:40.7	3.47 0.09	8.16 0.11	8.74 0.06	10.15 0.04	11.69 0.08	16.71 0.15	99.99 9.99	19.53 0.31	56.8	6.2	
TC4E	18:02:15.79-23:06:42.8	3.57 0.10	7.51 0.06	7.47 0.01	8.26 0.01	9.45 0.02	15.06 0.02	18.12 0.44	99.99 9.99	70.0	10	
TC1	18:02:24.68-23:01:17.7	2.02 0.90	8.87 0.55	9.19 0.17	9.70 0.06	10.68 0.11	17.24 0.35	17.91 0.29	19.43 0.27	–	19	
TC2	18:02:28.49-23:03:56.9	2.09 0.11	5.76 0.02	7.69 0.03	10.48 0.06	10.78 0.07	13.57 0.02	16.20 0.08	19.15 0.20	–	24	

<sup>a</sup>near-infrared data are from Palomar 200 inch measurements.

<sup>b</sup>separation of TC3B-TC3E from the central protostar TC3A in the TC3 core, and separation of TC4B-TC4E from the central protostar TC4A in the TC 4 core. for TC4 condensation.

<sup>c,d</sup> $_{mid-IR}$  is mid-infrared luminosity estimated from 1.2-24 $\mu$ m.

## REFERENCES

- André, P., 1994, *Protostars and Planets IV*, The University of Arizona press, ed. V. amnnings, A.P. Boss, S.S. Rus
- Bonnell I. A. & Davies, M. B., 1998, MNRAS, 295, 691
- Bonnell I. A. Vine, S. G. & Bate, M. R., 2004, MNRAS, 349, 735
- Cernicharo, J. et al., 1998, Science, 282, 462
- Cernicharo, J. et al., 2000, Science, 288, 649
- Draine, B. T., 2003, ApJ, 598, 1017
- Fazio, G. et al., 2004, ApJS, 154, 10
- Hester et al, 1999, BAAS, 194.681
- Indebetouw, R. et al., 2005, ApJ, 619, 931
- Indebetouw, R., Whitney, B.A. Johnson, K. E., Wood, K., 2005, ApJ, 636, 3621
- Lefloch, B. & Cernicharo, J., 2000, ApJ, 545, 340
- Lefloch, B., Cernicharo, J., Rodríguez, L.F., Miville-Deschénes, M.A., & Cesarsky, D., Heras, A., 2002, ApJ, 581, 335
- Lada, C., 1991, *The Physics of Star Formation and Early Stellar Evolution*, NATO Advanced Science Institutes (ASI) Series C, Vol. 342, Kluwer, 1991, edited by Charles J. Lada and Nikolaos D. Kylafis., p.329
- Li, A. & Draine, B. T., 2001, ApJ, 554, 778
- Lynds, B. T., & O'neil, E. J., Jr., 1985, ApJ, 294, 578
- McKee, C.F. & Tan J. C., 2002, Nature, 416, 59
- McKee, C.F. & Tan J. C., 2003, ApJ, 585, 850
- Muzerolle, J. et al., 2004, ApJS, 154, 379
- Nakano, T., Hasegawa, T., Morino, J.-I., & Yamashita, T., 2000, ApJ, 534, 976
- Noriega-Crespo, A., Moro-Martin, A., Carey, S., Morris, P. W., Padgett, D. L., Latter, W. B., & Muzerolle, J., 2004, ApJS, 154, 402
- Osorio, M., Lizano, S., & D'alessio P., 1999, ApJ, 525, 808
- Reach, W. T., Rho, J., et al. 2004, ApJS, 154, 385

- Reach, W. T. et al., 2005, *PASP*, 117, 978
- Rho, J., Corcoran, M.F, Chu, Y.-H., & Reach, W. T., 2001, *ApJ*, 562, 446
- Rho, J., Ramirez, S.V., Corcoran, M.F., Hamaguchi, K., & Lefloch, B., 2004, *ApJ*, 607, 904
- Rieke, G. et al., 2004, *ApJS*, 154, 25
- Shirley, Y. L., Evans, N. J., Young, K. E., Knez, C. & Jaffe, D. T., 2003, *ApJS*, 149, 375
- Williams, S.J., Fuller, G.A. & Sridharan, T.K., 2004, *A&A*, 417, 115
- Weingartner J. C. & Draine, B. T., 2001, *ApJ*, 548, 296
- Young et al., 2004, *ApJS*, 154, 396
- Yusef-zadeh, F., Shure, M., Wardle, M., Kassim, N., 2000, *ApJ*, 540, 842

Fig. 1.— Mosaicked three-color *Spitzer* image of the Trifid Nebula. Blue, green and red represent IRAC 4.5 and 8 $\mu$ m, and MIPS 24 $\mu$ m images, respectively. PAH-dominated emission appears in green, hot dust grains appear in red, and young stellar objects appear as point sources in red or yellow. Also note the filamentary dark clouds on the western side of M20. The diffuse emission at 8 and 24 $\mu$ m ranges between 80 and 450 MJy sr<sup>-1</sup>, and between 90 and 280 MJy sr<sup>-1</sup>, respectively. The image is centered at R.A. 18<sup>h</sup>02<sup>m</sup>26<sup>s</sup> and Dec. -23°00'39" (J2000), and covers an 18'×26' arcmin field of view. (*Fig. 1 is a jpeg file*)

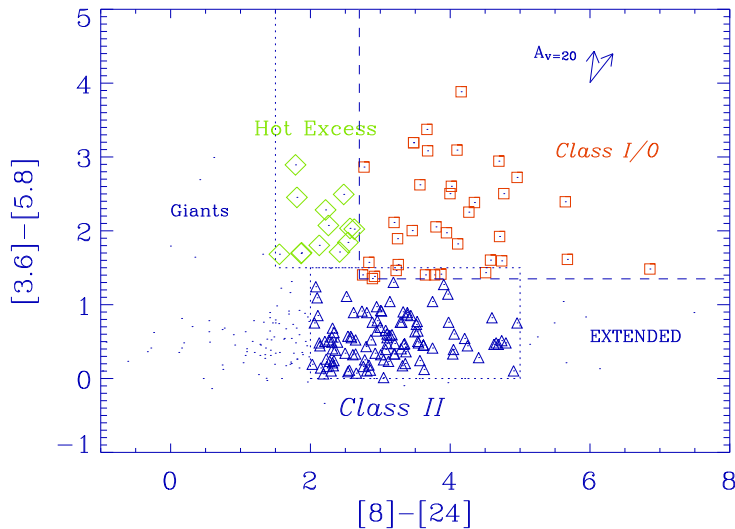


Fig. 2.— *Spitzer* color-color diagram in the Trifid Nebula, using IRAC and MIPS data. The approximate locations of Classes of I/0, II and “Hot excess” YSOs are outlined. Protostars of Classes I/0 are the reddest stars (squares) located in the upper right in this diagram, and evolved YSOs of Class II are red in the color of [8]-[24] and marked with triangles. The extinction vectors for  $R_v = 5.5$  (thin line) and  $R_v = 3.1$  (thick line) are shown as arrows, which are estimated based on Weingartner & Draine (2001). The extinction vector by using other set of *Spitzer* IRAC data (Indebetouw et al. 2005) is approximately consistent with the case of  $R_v = 5.5$ .

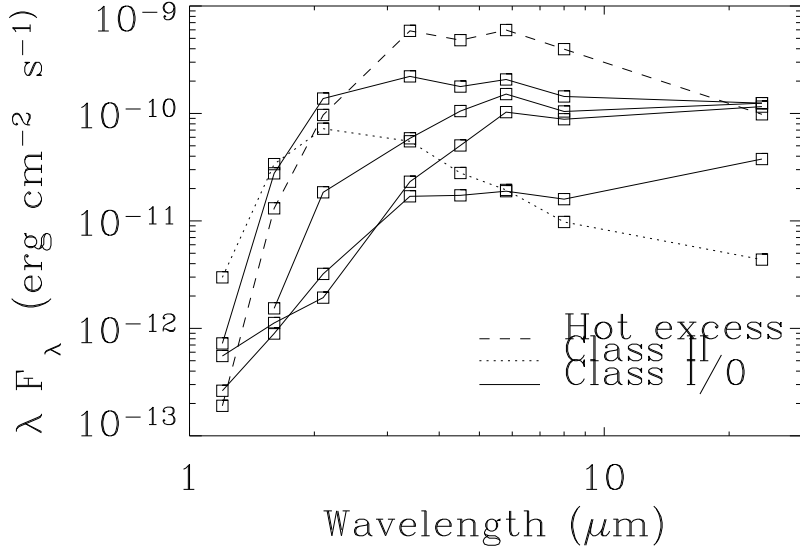


Fig. 3.— Examples of near- and mid-infrared spectral energy distributions of three different Classes of YSOs: Class I/0, Class II and “Hot excess” stars.

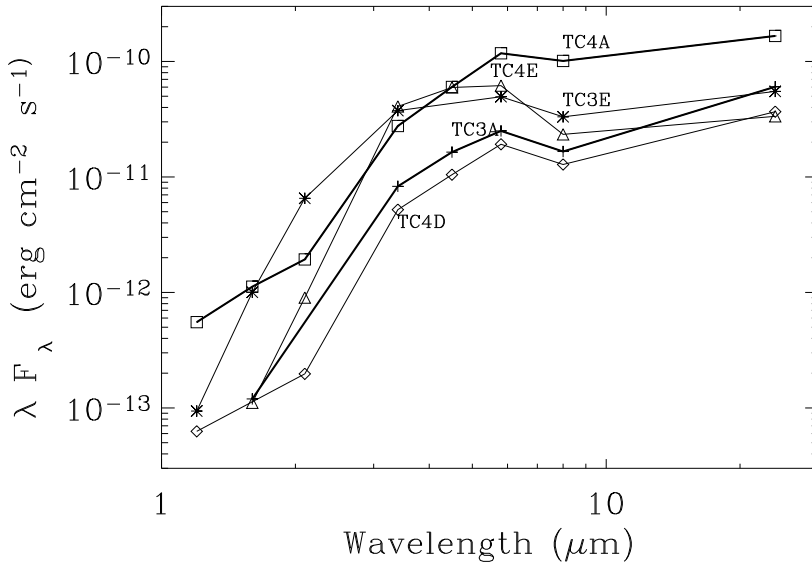


Fig. 4.— Near- and Mid-infrared spectral energy distributions of TC3A (crosses), TC3E (astericks), TC4A (squares), TC4D (diamonds), and TC4E (triangles). The sources show dips at 8 $\mu$ m, which is likely due to silicate absorption feature.

Fig. 5.— Comparison of the HST (on left) and *Spitzer* IRAC (on right) images of the Trifid Nebula. While the protostars appear dark in the optical HST image, they appear as infrared color excess stars (yellow or green) in the *Spitzer* images. Four condensations are marked as circles for TC1 (top) and TC2 (middle), and ellipses for TC3 (bottom right) and TC4 (bottom left), and the protostars within the cores are marked as arrows. Four of the five protostars within each of TC3 and TC4 cores are marked, because they are clearly noticeable in the IRAC color images; all five protostars are shown in Figure 6 (see the text for details). North is up and west is to the right. (*Fig. 5 is a jpeg file*)

Fig. 6.— A portion of the *Spitzer* color image (from Fig. 1) superposed on 1300 $\mu$ m contours from Lefloch & Cernicharo (2000). The contour levels are 5, 10, 15, 20, 30, 45, 60 by 30, 200 to 350 Jy by 50 mJy beam $^{-1}$ , where the beam size is 11". Class I/0 sources are marked as green circles, and Class II and “hot excess” sources are marked as red and white circles. The TC3 and TC4 mm sources are each associated with multiple protostars. The brightest protostars appear near the centers of the dust continuum peaks. (*Fig. 6 is a jpeg file*)

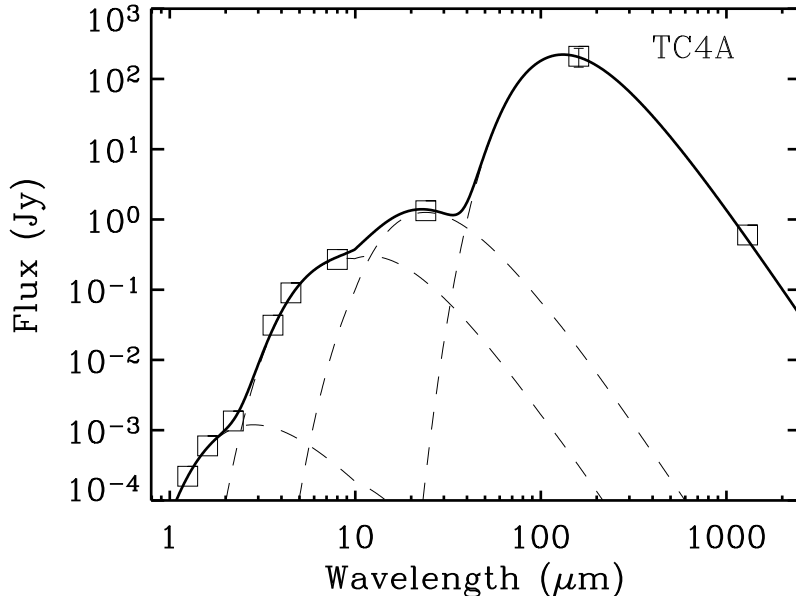


Fig. 7.— Broad band spectral energy distribution of TC4A, the most massive protostars of TC4. The best-fit black body model with four temperatures of  $T_{cold}=22$  K,  $T_{warm}=150$  K,  $T_{hot1}=400$  K, and  $T_{hot2}=1300$  K is shown.

This figure "f1.jpg" is available in "jpg" format from:

<http://arxiv.org/ps/astro-ph/0601633v1>

This figure "f5.jpg" is available in "jpg" format from:

<http://arxiv.org/ps/astro-ph/0601633v1>



This figure "f6.jpg" is available in "jpg" format from:

<http://arxiv.org/ps/astro-ph/0601633v1>